PAPER

Check for updates

Algal biomass from the stable growth phase as a potential biosorbent for Pb(II) removal from water

Yinta Li, [ID][abc] Ling Xia,*[ad] Rong Huang,[a] Chenggong Xia[a] and Shaoxian Song*[ad]

In this study, the effect of the growth phase on the Pb(II) removal performance from water using *Chlorella* sp. QB-102 dry biomass was investigated. Optimum biosorption conditions were determined as a function of initial solution pH and contact time. Freundlich isotherm and pseudo-second-order kinetics models were found to be most applicable to Pb(II) adsorption on biomass from each growth phase. The maximum adsorption capacities of Pb(II) were found to be 205.5, 298.5 and 171.9 mg g^{-1} for logarithmic, stable and decline phases of biosorbents, respectively. The FT-IR, XPS and potentiometric titration results showed that the lack of phosphoryl groups caused the lowest adsorption efficiency for the decline phase, and the more effective active sites in carboxyl and higher site concentrations of hydroxyl and phosphoryl functional groups led to most of the bioadsorption occurring during the stable phase. Thus, algal biomass from the stable phase can be used as a potential adsorbent for heavy metal removal from water.

1 Introduction

With the rapid development of industrialization, plenty of industrial effluents containing heavy metals are discharged into unpolluted natural water bodies.[1,2] These heavy metals can be accumulated in living organisms, including humans, animals and plants. Unlike organic pollutants, heavy metals are non-biodegradable and remain in the environment available to cause pollution.[1,3] Lead is one of the common contaminants, which causes various health hazards. It is harmful to nervous, digestive, blood, endocrine and reproductive systems.[2] Therefore, the permissible limit of lead in potable water should not exceed 0.01 mg L^{-1} according to the regulation of the WHO.

Conventional methods for heavy metal removal from wastewater include chemical precipitation, complexation, ion exchange, reverse osmosis, filtration, and coagulation. Nevertheless, these processes are limited by high capital and operational cost.[1,4] Biosorption has emerged as a potential alternative to conventional methods for the heavy metals removal due to its cost effectiveness, high selectivity and efficiency, and good removal performance.[5] In the last decades, different sources of biomass, such as bacteria, fungi, and algae have been screened and studied extensively.[1,6,7] Among them, algae including macroalgae and microalgae have been proven to be highly effective, reliable and predictable in the heavy metals removal from aqueous solutions.[6,8–10] It has been found that algal biomass are rich in organic ligands or functional groups, such as carboxyl, hydroxyl, phosphate, amine groups, and so on. These functional groups play dominant roles in the heavy metals removal. However, most researches mainly concern the potential of algal biomass as adsorbents for heavy metal removal, or the modification of algal biomass for better biosorption of heavy metals.[6,8–10] Well, with the growth time of algal cells, the biochemical component and also surface properties as well as the biomass concentration from different growth phases can be changed. To the best of our knowledge, there are rare reports focus on the effect of growth phase on the surface properties of algal biomass and further effect on the removal performances of heavy metal.

The objective of this study was to screen the best harvest stage for algal biomass as adsorbent for efficient lead removal from water. *Chlorella* sp. QB-102, isolated form a lead–zinc tailing wasteland was selected as the research subjective. The study gave detailed analysis of lead adsorption behaviors on algal dry biomass from different growth stages in terms of adsorption isotherms and kinetics experiments. Meanwhile, the effect of growth stage on biomass surface characterization has been investigated. The explanations for adsorption mechanism have been supported by FT-IR, XPS and potentiometric titration.

2 Materials and methods

2.1 Algal-based adsorbents preparation

Chlorella sp. QB-102 was isolated from the tailing wasteland in Qibo mountain lead–zinc mine, Shanggao, Jiangxi provence in

[a]School of Resources and Environmental Engineering, Wuhan University of Technology, Luoshi Road 122, Wuhan, Hubei, 430070, China. E-mail: xialing@whut.edu.cn; ssx851215@whut.edu.cn

[b]Doctorado Institucional de Ingeniería y Ciencia de Materiales, Universidad Autonoma de San Luis Potosi, Av. Sierra Leona 530, San Luis Potosi, C.P. 78210, Mexico

[c]Department of Food Engineering, Weihai Ocean Vocational College, Haiwan South Road 1000, Weihai, Shandong, 264300, China

[d]Hubei Key Laboratory of Mineral Resources Processing and Environment, Luoshi Road 122, Wuhan, Hubei, 430070, China
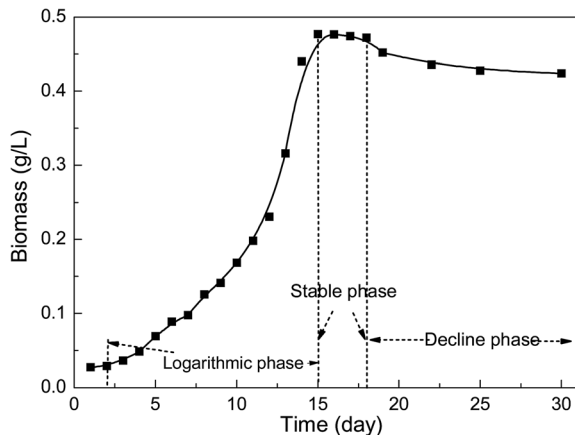
Fig. 1 The growth curve of *Chlorella* sp. QB-102 in the BG-11 medium.

China (28°09′N, 114°52′E) and identified by classical morphological methods. Stock cultures were grown in BG-11 medium containing 1.5 g $NaNO_3$, 30 mg K_2HPO_4, 36 mg $CaCl_2 \cdot 2H_2O$, 6 mg ammonium citrate monohydrate, 6 mg ammonium ferric citrate, 1 mg EDTA, 2.86 μg H_3BO_3, 1.81 μg $MnCl_2 \cdot 4H_2O$, 0.222 μg $ZnSO_4 \cdot 7H_2O$, 0.39 μg $NaMoO_4 \cdot 5H_2O$, 0.079 μg $CuSO_4 \cdot 5H_2O$, 0.050 μg $CoCl_2 \cdot 6H_2O$ in 1 L sterile distilled water.[11]

For trials, *Chlorella* sp. QB-102 cells were cultivated in BG11 medium at 25 °C with a light/dark cycle of 14 h/10 h. Samples were taken every day to measure the biomass concentration. The biomass from exponential (day 14), stable (day 18) and declined phase (day 29) as presented in Fig. 1 was centrifuged harvested, washed three times and then freeze-dried (FD-1B-50, Ouman International Industry Co., Ltd., China) for the subsequential biosorption experiments.

2.2 Reagents

A stock solution containing 1000 mg L^{-1} Pb(ɪɪ) was prepared by $Pb(NO_3)_2$ in deionized water. All chemicals were of analytical grade and obtained from the Xinyang chemical reagent (China). The pH of the test solution was adjusted with 0.1 M HNO_3 or 0.1 M NaOH. Deionized water was used throughout this study (Millipore Q, USA).

2.3 Biosorption experiments

The adsorption experiments of Pb(ɪɪ) were implemented in triplicate in 100 mL Erlenmeyer flasks with 50 mL of Pb(ɪɪ) solution combined with 10 mg of adsorbents in a mechanical shaker at the speed of 180 rpm at 25 °C. The influence of pH on Pb(ɪɪ) adsorption was conducted within a pH range of 2 to 6 at an initial Pb(ɪɪ) concentration of 100 mg L^{-1} for 6 h. Biosorption isotherm experiments were performed by ranging the initial concentration of Pb(ɪɪ) from 10 to 300 mg L^{-1} at pH 5.5 for 6 h. The kinetic experiments were studied by varying contact time intervals in the range of 0.5–300 min at an initial Pb(ɪɪ) concentration of 100 mg L^{-1} at pH 5.5. Afterwards, the mixture was filtered through 0.22 μm filter membrane and the supernatant was used for Pb(ɪɪ) determination.

2.4 Analytical methods

2.4.1 Biomass measurement. Generally, the dried cell weight of microalgae is correlated to the optical density (OD) at certain wavelength from 450 to 680 nm.[12] In this study, the biomass concentration (BC, g L^{-1}) of *Chlorella* sp. QB-102 was determined by measuring the optical density of 680 nm (OD_{680}) *via* an ultraviolet photospectrometer (Shimadzu UV-2550, Japan) as following eqn (1).

$$BC = 0.255 \times OD_{680} \ (R^2 = 0.9986) \qquad (1)$$

2.4.2 Pb(ɪɪ) determination. The concentration of Pb(ɪɪ) was determined using an atomic absorption spectrometry (ZEEnit700, Analyjena, Germany) at 283.3 nm. The biosorption capacity of Pb(ɪɪ) was calculated by the following eqn (2):[13]

$$q_e = \frac{V(C_0 - C_t)}{M} \qquad (2)$$

where q_e (mg g^{-1}) is the equilibrium biosorption capacity of Pb(ɪɪ); C_0 (mg L^{-1}) and C_t (mg L^{-1}) are the initial and final concentrations of Pb(ɪɪ), respectively; V (L) is the volume of mixture; M (g) is the weight of the adsorbent.

2.4.3 Zeta potential measurement. A Malvern Zetasizer Zeta-Nano (England) working with laser doppler electrophoresis technique was employed to determine the zeta potentials of the biosorbents as a function of pH within 2 to 7.

2.4.4 XPS analysis. The XPS spectrum (PHI-3056, PerkinElmzr, US) was used to analysis the adsorbents before and after Pb(ɪɪ) loading.

2.4.5 Potentiometric titration. Potentiometric titration (PT) was used to determine the deprotonation constants and absolute concentrations of the specific functional groups present on the algal cell walls.[14] The potentiometric measurements were performed at 25 ± 0.3 °C by a glass electrode (Sartorius pH meter, Germany). The suspension pH was firstly acidified to 2.5 under constant magnetic stirring (150 rpm). Then titration was performed by stepwise addition of 0.01 mL of 0.1 M NaOH to the cell and titrated up to pH 10 while the suspension was stirred under nitrogen protection. Titration data were fitted using a software Profit 2.1 based on the Donnan Shell Model.[15,16]

2.5 Isotherm and kinetics modelling

Langmuir (eqn (3)),[17] Freundlich (eqn (5))[18] and Temkin (eqn (6))[13] models were used to fit the biosorption data.

$$q_e = \frac{q_{max} K_L C_e}{1 + K_L C_e} \qquad (3)$$

where C_e (mg L^{-1}) is the equilibrium concentration of Pb(ɪɪ) solution; q_e (mg g^{-1}) and q_{max} (mg g^{-1}) are the amount of Pb(ɪɪ) equilibrium adsorbed capacity and the maximum monolayer biosorption capacity of Pb(ɪɪ), respectively; K_L (L mol^{-1}) represents the Langmuir model constant which related to the heat of biosorption.

R_L, a dimensionless constant as separation factor or equilibrium parameter, can determine whether the essential

biosorption characteristics of the Langmuir isotherm is favorable or unfavorable, defined as following:[17]

$$R_L = \frac{1}{1 + K_L C_0} \quad (4)$$

where C_0 (mg L^{-1}) is the highest initial concentration of Pb(II). R_L indicates the type of Langmuir isotherm to be irreversible ($R_L = 0$), favorable ($0 < R_L < 1$), linear ($R_L = 1$) or unfavorable ($R_L > 1$).

$$q_e = K_F C_e^{1/n} \quad (5)$$

where K_F (mol^{1-n} L^n g^{-1}) represents the biosorption equilibrium constant related to the biosorption capacity; n represents a constant related to the biosorption intensity to be good ($2 < n < 10$), moderately difficult ($1 < n < 2$), poor sorption characteristics ($n < 1$).[3]

$$q_e = A + B \ln C_e \quad (6)$$

where A (mg g^{-1}) and B (J mol^{-1}) are the Temkin constants.

The kinetic parameters were evaluated by using the pseudo-first order (eqn (7)),[19] pseudo-second-order (eqn (8)),[20] intra-particle diffusion (eqn (9))[21] models, the initial sorption rate (eqn (10)) and the half-sorption time (eqn (11))[22,23] expressed as follows:

$$\ln(q_e - q_t) = \ln q_e - k_1 t \quad (7)$$

$$\frac{t}{q_t} = \frac{1}{k_2 q_e^2} + \frac{t}{q_e} \quad (8)$$

$$q_t = C + k_n t^{0.5} \quad (9)$$

$$h = k_2 q_e^2 \quad (10)$$

$$t_{1/2} = \frac{1}{k_2 q_e} \quad (11)$$

where q_t (mg g^{-1}) represents the amount of Pb(II) adsorbed at time t (min), q_e (mg g^{-1}) represents the biosorption capacity at equilibrium time, k_n represents the rate constant of intra-particle diffusion, k_1 (min^{-1}) and k_2 (g mg^{-1} min^{-1}) represents the rate constants for pseudo-first-order and pseudo-

second-order, respectively, h (mg g^{-1} min^{-1}) represents the initial sorption rate of Pb(II), $t_{1/2}$ (min) represents the time needed to adsorb half of the equilibrium value of Pb(II).

3 Results and discussion

3.1 Influences of growth phase on Pb(II) biosorption

3.1.1 Effect of initial solution pH. pH not only affects the dissociation degree of functional groups on biomass surface but also the speciation and solubility of metal ions, and further affects the uptake capacity of metal ions onto the biomass.[23] In this study, the initial solution pH was adjusted within a range from 2.0 to 6.0 to investigate the effect of pH on Pb(II) adsorption as presented in Fig. 2a. It showed that the biosorption capacity of Pb(II) on algal biomass increased with increasing pH, and the retention of Pb(II) is highest at pH of 5.5 for the algal biomass from all three growth phases. After this pH value, the biosorption capacity decreased as the pH increases for all cases, which may be caused by the change of the speciation of lead during the secondary hydrolysis processes.[6] It was also noted that within the studied pH range, algal dry biomass from stable phase showed the highest adsorption capacity, followed by exponential and declining phases.

Fig. 2b shows the zeta potential of algal biomass from three growth phases as a function of pH. The zeta potential of algal biomass from all the growth phases was negatively charged within the pH range from 2.0 to 7.0, and the net zeta potential increased with pH increasing. Thus, at pH 2.0 where the ionization degree of superficial functional groups of biomass in terms of zeta potential is lower, the biosorption capacity of Pb(II) was lower. Meanwhile, the increase in the initial solution resulted in the increase of net negatively charged biomass surface, in consequence the number of electrostatic interactions increased. The stable phase biomass showed the lowest net negative surface charge when pH was above 2, which can explain that the lowest biosorption capacity of Pb(II) compared with that from other two growth phases. In addition, at pH values higher than 5.5, the decrease in biosorption capacity probably due to conversion of Pb(II) ions to hydroxylated complexes of Pb(II), resulting into hydroxide precipitation.
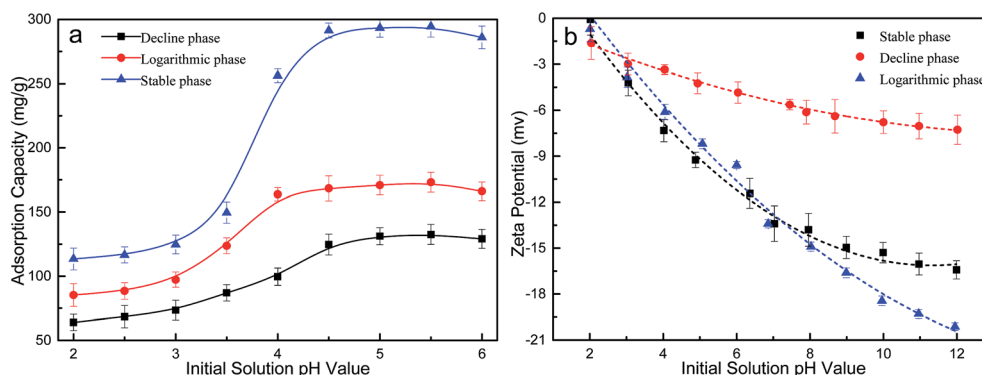

Fig. 2 The effect of the initial solution pH values on the adsorption capacity (a) and zeta potential as a function of pH (b) of dried *Chlorella* sp. QB-102 biomass of each growth phase (initial Pb(II) concentration of 100 mg L^{-1}, 25 °C).
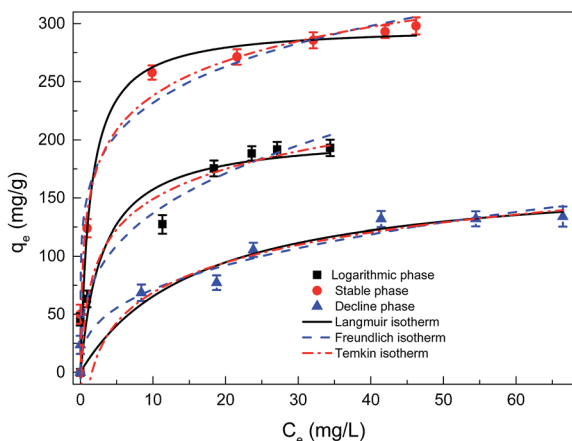
Fig. 3 Adsorption isotherms of dried *Chlorella* sp. QB-102 biomass of each growth phase, the experimental data were fitted with Langmuir, Freundlich and Temkin models (25 °C, pH 5.5 for 6 h).

Consequently, an initial solution pH of 5.5 was considered as the optimum value and was used in all the following experiments.

3.1.2 Biosorption isotherm. The biosorption isotherm models are useful for expressing the surface properties and metal binding behaviors of biosorbent. In this study, three isotherm models were selected to fit the experimental data, namely Langmuir, Freundlich and Temkin models. Fig. 3 illustrates the adsorption capacity of Pb(II) on dried *Chlorella* sp. QB-102 biomass from three growth phases as a function of initial Pb(II) concentration. The biosorption capacities of algal biomass from all the growth phases increased with increasing Pb(II) equilibrium concentration until reached plateaus. These data were further fitted to Langmuir, Freundlich and Temkin models, and the results were given in Table 1. These results all suggested that the biosorption isotherm of Pb(II) onto the dried *Chlorella* sp. biomass of each growth phase belonged to the Freundlich model in terms of the highest linear regression coefficient (R^2). Freundlich isotherm data showed multilayer deposition of lead ion species on algal surface.[6,24]

As shown in Table 1, the K_F value (153.1 L g^{-1}) of Pb(II) adsorbed on the dried *Chlorella* sp. QB-102 biomass from stable phase was significantly higher than that from logarithmic phase (61.8 L g^{-1}) or decline phase (30.7 L g^{-1}). Correspondingly, the highest maximum biosorption capacity was also obtained at stable phase from Langmuir fitting, valued at 298.2 mg g^{-1}, which was 1.5 times higher against that at exponential phase (205.5 mg g^{-1}) and 1.8 times against that at declining phase

(171.9 mg g^{-1}). The largest biosorption capacity was higher than most biosorbents as listed in Table 2. These results indicated that the biomass from stable growth phase showed the best performances as an adsorbent for Pb(II) removal from water.

3.1.3 Biosorption kinetics. The adsorption capacity of Pb(II) on dried *Chlorella* sp. QB-102 biomass from three growth phases as a function of time were studied and shown in Fig. 4a. At each growth phase, the Pb(II) biosorption efficiency increased rapidly and more than 85% of biosorption was accomplished within 5 min. Then, the biosorption capacity increased slowly until 30 min and further increasing time to 300 min showed no obvious changes due to the decreasing number of biosorption sites available on the biosorbent surface. As expected, the biosorption capacity of Pb(II) on dried stable stage biomass was the highest at any time during the biosorption process compared to the exponential or decline stages.

The experimental data were further fitted to the pseudo-first-order, pseudo-second order and intra-particle diffusion models. Linear plots of log ($q_e - q_t$) *versus* t, t/q_t *versus* t and q_t against $t^{0.5}$ were illustrated in Fig. 4b–d, and the associated kinetic parameters and the corresponding linear regression R^2 were summarized in Table 3. It showed that the experimental data were best fitted with the pseudo-second-order model according to R^2 for biomass from all three growth phases. It was suggested that the biosorption of Pb(II) on the algal biomass was chemisorption.

In addition, it was worth mentioning that the biosorptive capacity of Pb(II) on dried *Chlorella* sp. QB-102 biomass of the stable phase is faster than those of the logarithmic and decline phase based on the h and $t_{1/2}$ values (Table 3). The h and q_e values of dried *Chlorella* sp. QB-102 biomass of the stable phase were more than 3 times and 1.5 times higher than those of the logarithmic and decline phase, respectively.

Given that the algal biomass from stable phase for Pb(II) removal showed the best performances in terms of higher biosorption capacity and shorter reaction time, it was recommended that the harvesting operation can be implemented when the algal cells grow to a stable stage when using as algal-based adsorbents.

3.2 FT-IR spectroscopy

The FT-IR spectra of biosorbents from three growth stages are shown in Fig. 5a. The broad and intense adsorption band at around 3303 cm^{-1} was attributed to the bending vibration of the water molecule and –OH stretching frequency in carbohydrates, protein and lipids.[4] The peaks at around 2924 and 1458

Table 1 Langmuir, Freundlich and Temkin constants related to the adsorption isotherms of Pb(II) onto dried *Chlorella* sp. QB-102 of each growth phase

	Langmuir			Freundlich			Temkin		
	q_e (mg g^{-1})	K_L (L g^{-1})	R^2	K_F (L g^{-1})	$1/n$	R^2	A	B	R^2
Logarithmic phase	205.5	0.326	0.9672	64.83	0.324	0.9729	60	37.55	0.8715
Stable phase	298.2	0.738	0.9912	153.13	0.181	0.9957	100	42.56	0.8939
Decline phase	171.9	0.061	0.9761	30.71	0.367	0.9861	−20	37.35	0.8861

Table 2 Comparison of the adsorption capacity of Pb(II) in this study with other biosorbents

| Adsorbent	pH	Adsorption capacity (mg g^{-1})	Contact time	References
Pelvetia canaliculata	5.0	300.1	100 h	(Costa, Vilar, Botelho, da Silva, & Boaventura, 2010)
Algal strains	3.0–5.0	50–208	30 min	(Romera, González, Ballester, Blázquez, & Muñoz, 2007)
Sargassum sp.	5	240.3	60 min	(Sheng, Ting, Chen, & Hong, 2004)
Lactarius scrobiculatus	5.5	56.2	60 min	(Anayurt, Sari, & Tuzen, 2009)
Ulva sp.	5	287.6	60 min	(Sheng *et al.*, 2004)
Bacillus sp. L14	5.0–5.5	280.02	5 min	(Luo *et al.*, 2014)
Cabbage waste	6.0–6.5	40.963–50.216	3 h	(Hossain *et al.*, 2014)
Fe$_3$O$_4$-treated waste litchi peel	6.0	78.74	120 min	(R. Jiang *et al.*, 2015)
Chlorella sp. QB-102	5.5 ± 0.3	297.1	5 min	This study
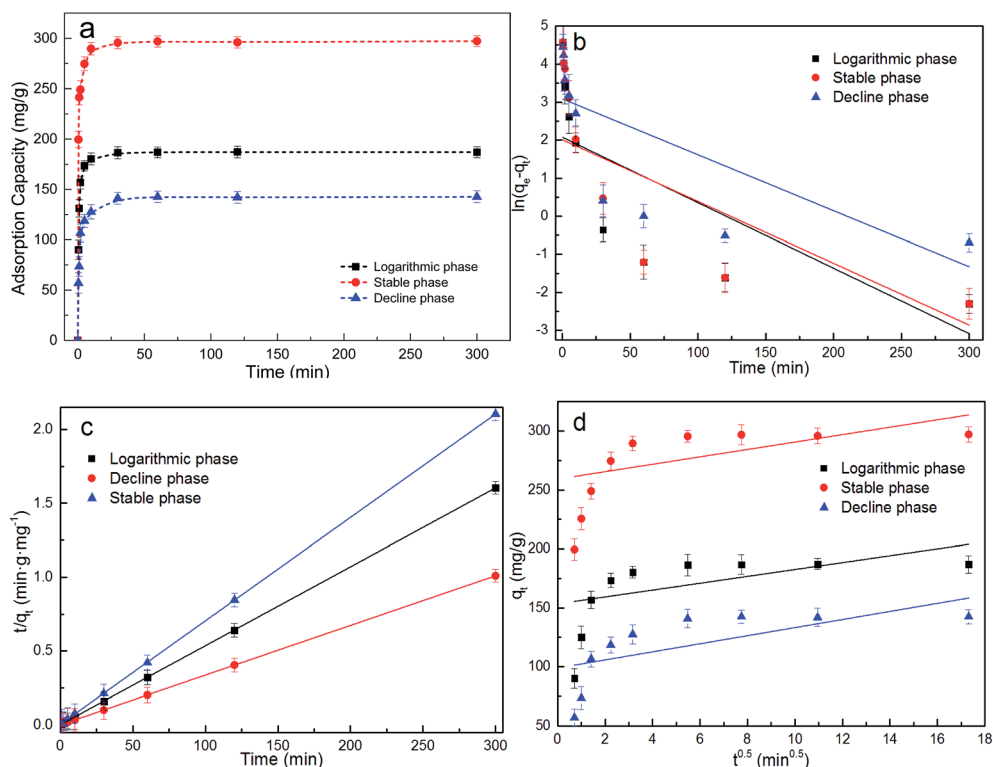
Fig. 4 Effect of contact time on the Pb(II) adsorption capacity on biomass of each growth phase (a). The pseudo-first-order model (b), pseudo-second-order model (c), and intra-particle diffusion model (d) sorption kinetics curves were fitted with experimental data (initial Pb(II) concentration of 100 mg L^{-1}, 25 °C, pH 5.5 for 6 h).

cm^{-1} were assigned to the asymmetric stretching bands of carboxylates groups.[20] The peaks at 1610–1634 cm^{-1} was assigned to C=C stretching mode from peptide of amide I.[25] The above functional groups were all present in the biosorbents from the three growth stages. However, it was worth mentioning that the characteristic features were the peaks at 1248 and 1080 cm^{-1} only presented in the biomass from logarithmic and stable phases, attributed to the P=O stretching bands.[15,26]

After biosorption of Pb(II), the broad peaks shifted from 3387 to 3405 cm^{-1} for the biomass from all three growth phases, which might be attributed to the complexation of Pb(II) with free or bonded –OH groups (Fig. 5b–d). The variation in peaks at 1744 and 1247 cm^{-1} in algal biomass of logarithmic growth phase represented –C=O groups in carboxylic acids and phosphate groups stretching vibration due to complexation of Pb(II) with these sites. As for the stable phases, besides variations of –C=O and –P=O groups, a shift of peak at 1458 cm^{-1} was observed, which considerably might be due to the complexation between Pb(II) and –COOH groups. In contrast, the decline phase lacking phosphate groups showed a variation peaks located at 1623 and 1428 cm^{-1}, which might be attributed to the reaction between Pb(II) with –C=O and –COOH groups. It can

Table 3 Parameters of pseudo-first-order, pseudo-second-order, intra-particle diffusion models

|	Pseudo-first-order kinetics				Pseudo-second-order kinetics					Intra-particle diffusion model		
	$q_{e,exp}$ (mg g^{-1})	$q_{e,cal}$ (mg g^{-1})	k_1 (min^{-1})	R^2	$q_{e,cal}$ (mg g^{-1})	k_2 (min^{-1})	R^2	h (mg g^{-1} min^{-1})	$t_{1/2}$ (min)	K_n (mg g^{-1} min^{-1})	C	R^2
Logarithmic phase	187.1	182.3	1.222	0.6736	188.8	0.0111	1	395.6	0.4772	16.55	12.074	0.2294
Stable phase	297.1	287.8	2.001	0.7217	295.7	0.0128	1	1119	0.2642	25.63	19.71	0.2722
Decline phase	142.5	136.7	0.813	0.6970	142.6	0.0088	1	179.0	0.7968	11.47	7.51	0.3841
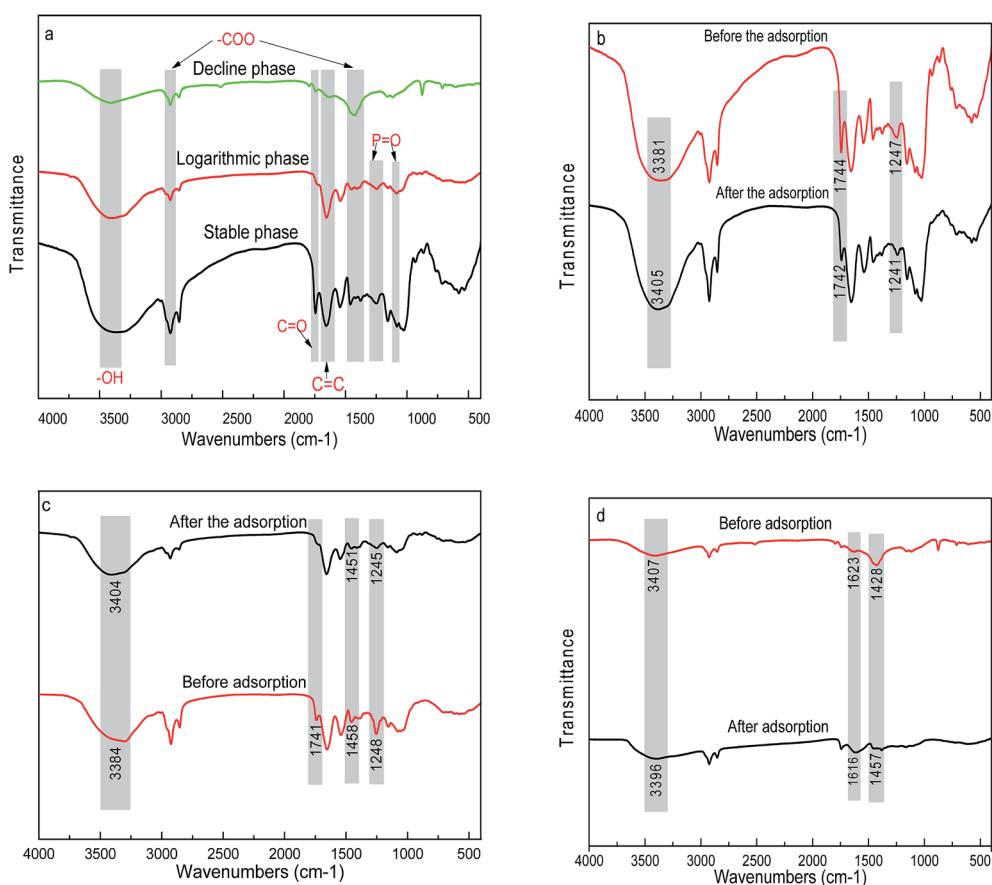
Fig. 5 FT-IR spectra of dried *Chlorella* sp. QB-102 of each growth phase (a) before adsorption as well as dry biomass of logarithmic phase (b), stable phase (c) and decline phase(d) before and after Pb(ɪɪ) loaded.

be concluded that the growth stages significantly influenced the surface functional groups of algal biomass, which can be attributed to the gradually depletion of the nutrients in the medium with the cultivation time of the serial growth phases. The changes in the functional groups at different growth phases further affected the biosorption capacity of heavy metals.

3.3 X-ray photoelectron spectroscopy

To further explore the Pb(ɪɪ) biosorption mechanism, the biomass of dried *Chlorella* sp. QB-102 at three growth phase before and after Pb(ɪɪ) loading were analyzed by XPS and shown in Fig. 6. It can be seen from Fig. 6a, the main compositions of the biosorbents for all three stages were C, O and N, however, P

for only stable and decline phase, which was consistent with the observation in FT-IR (Fig. 6a). After Pb(ɪɪ) was adsorbed, two new peaks appeared at the binding energy of 141.4 eV and 136.2 eV for all the samples, which belonged to Pb 5s and Pb 4f, respectively.[27] Hence, it can be concluded that Pb was successfully absorbed onto the surface of biomass from all three growth stages.

The high-resolution XPS spectra of C 1s and O 1s for dried *Chlorella* sp. QB-102 biomass of each growth phase before and after Pb(ɪɪ) biosorption was shown Fig. 6b and c, respectively. As summarized in Table 4, C1 peaks were resolved into the following components peaks: and C–C and C–H, around 284 eV; C–C=O and C–OH, around 286 eV; O=C–OR and O=C–OH,
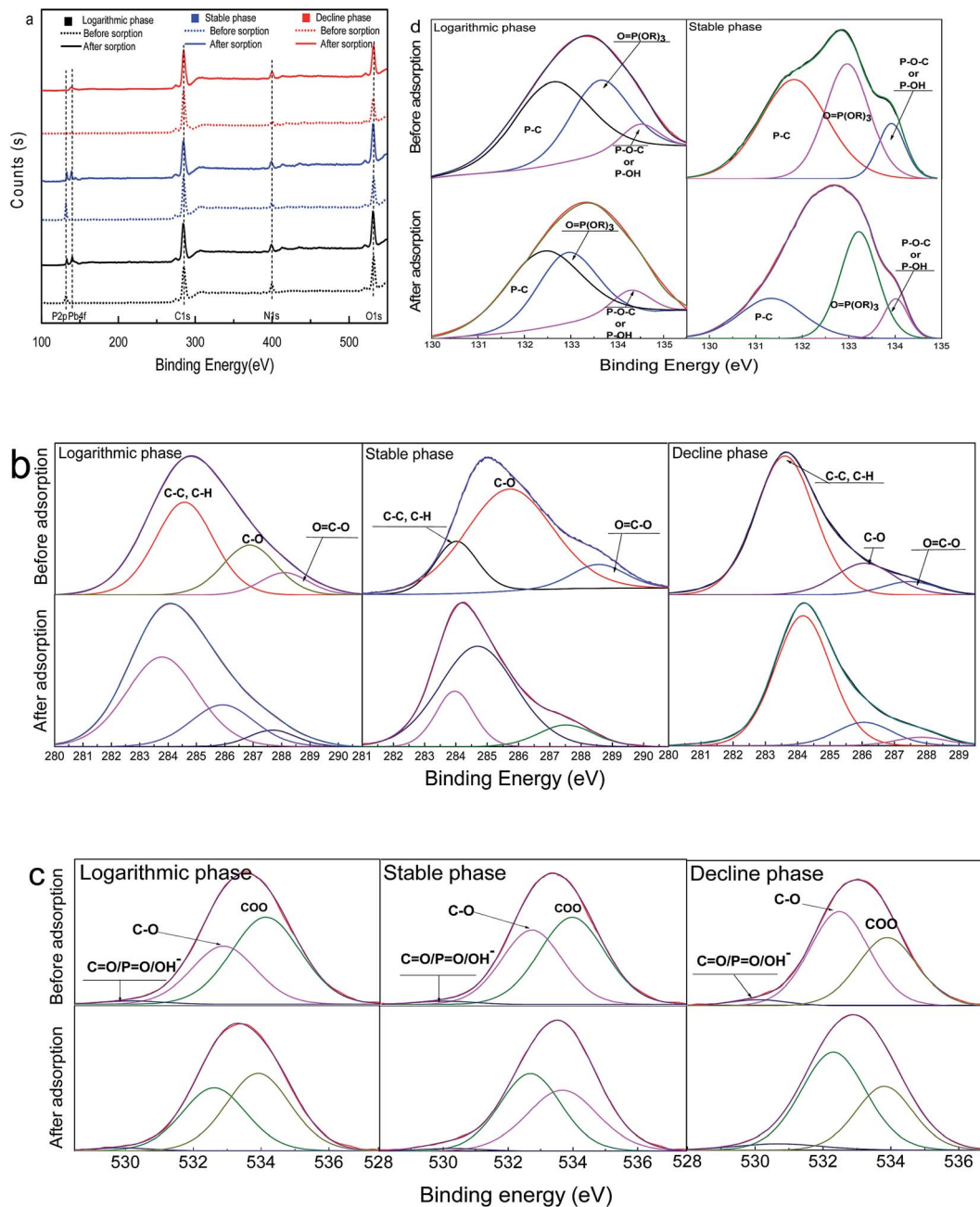
Fig. 6 XPS spectra of dried *Chlorella* sp. QB-102 biomass of each growth phase (a) as well as the high-resolution XPS spectra of C 1s (b) and O 1s (c) of biomass of each growth phase and P 2p of logarithmic and decline phases (d) before and after Pb(II) adsorption.

around 287 eV. O1 peaks were also resolved into three component peaks: the small peak at around 529 eV represented O=P–O⁻ or O=C–O⁻ from phosphate or carboxylate; the strong peak at around 532 eV was associated with C–O–(C, H, P) in alcohols, acetal, or esters; and the peak at around 534 eV was attributed to C–O (carboxyl and ether).[28–30] In addition, the intensity of carbon peak was considerably decreased while oxygen peak was increased on surface of the metal loaded biosorbents of each growth phase. The quantity of C in C–C=O/C–OH and O=C–OR/O=C–OH was considerably decreased for the biosorbents of each growth phase after Pb(II) was adsorbed, so did the quantity

of O in O=P–O⁻/O=C–O⁻. The shift in the binding energies and the decreased area ratio in these groups after Pb(II) biosorption for the samples of each growth stage was likely to be caused by the binding of lead ions onto the oxygen atoms. It was worth mentioning that the carboxyl groups (COO⁻) at around 534 eV was found decreased in the biosorbent-Pb(II) of stable and decline phase, however, not the logarithmic phase. The observation was consistent with the results of FT-IR.

Fig. 6d was the P 2p XPS spectra for the samples from logarithmic and stable phases before and after Pb(II) loading. It was noted that both intensity and relative area of P 2p obviously

Table 4 Summary of binding energies for the adsorbents

| | | Logarithmic phase | | | | Stable phase | | | | Decline phase | | | |
| | | Biomass | | Biomass + Pb(II) | | Biomass | | Biomass + Pb(II) | | Biomass | | Biomass + Pb(II) | |
		E_B (eV)	%	E_B (eV)	%	E_B (eV)	%	E_B (eV)	%	E_B (eV)	%	E_B (eV)	%
C 1s	C–C=O/C–OH	286.4	31.83	286.1	20.31	285.6	41.72	285.1	23.67	286.5	17.31	286.3	10.38
	O=C–OR/O=C–OH	287.9	12.79	287.7	9.46	288.2	11.30	287.6	7.22	288.3	6.82	288.0	4.11
O 1s	C=O/P=O/OH–	529.7	2.91	529.7	1.27	529.8	4.90	529.6	2.87	529.9	4.84	530.2	3.51
	C–O	532.8	43.41	532.6	44.52	532.6	42.54	532.5	47.09	532.5	63.53	532.3	67.63
	COO⁻	534.0	54.68	534.1	52.21	533.8	53.56	533.8	46.04	534.2	32.63	534.0	30.86
P 2p	P–C	132.5	27.28	132.4	15.97	131.7	40.91	131.3	13.57				
	O=P(OR)₃	133.6	11.66	133.6	8.65	133.3	42.05	133.3	12.99				
	P–O–C/P–OH	134.51	5.29	134.47	2.19	134.11	17.04	134.0	5.83				

decreased after biosorption of Pb(II). It was observed that after Pb(II) adsorption, the position of P 2p peak shifted to a lower energy, reducing by 0.89 and 0.80 eV respectively for logarithmic and stable phases, indicating that the relevant chemical reaction occurred between Pb(II) and the biosorbents from stable and decline growth phase during the biosorption process. The P 2p spectra can be decomposed into three components 131.50, 133.00 and 134.20 eV, which can be assigned to P–C, O=P(OR)₃ and P–O–C (phosphate),[31–33] respectively. The relative area ratio of the three P-binded functional groups considerably reduced for the biosorbents from both exponential and stable phases after Pb(II) was adsorbed, indicating that all the phosphorus functional groups involved in the complexation reactions with Pb²⁺.

3.4 Potentiometric titration

The species and concentrations of functional groups on the surface of dried *Chlorella* sp. QB-102 biomass of each growth phase were determined by PT. The pK values, site densities (mol kg$_{dw}$$^{-1}$) and corresponding functional groups were summarized in Table 5. The first pK was attributed to the carboxyl groups (pK = 2–6).[14,15] The pK_2 and pK_3 were at around pH 6.7 and pH 8.7, which can be attributed to the phosphoric (pK = 5.6–7.2) and amine groups (pK = 8.6–9.0) that exist in the form of bioorganic molecules on the cell wall of microalgae. The pK_4 appeared at around pH 10 and this buffering capacity is usually attributed to hydroxyl functional groups on the algal surface. The predominant functional groups for three growth phases observed were in agreement with the result of FT-IR, and they are all the active

sites for Pb(II) binding. It was worth noted that the phosphoryl functional groups were not found in biomass of decline phase, which was consistent with the observations of FT-IR and XPS. It might be because the depletion of phosphorus after the long-time incubation during the decline phase.

For the four sites, the binding site densities were estimated to be 0.39, 0.19, 0.21 and 2.95 mol kg^{-1} for logarithmic phase; 0.27, 0.22, 0.23, 3.07 mol kg^{-1} for stable phase, respectively. While for the decline phase, 0.15, 0.22, 1.81 mol kg^{-1} for carboxyl, amine and hydroxyl functional groups, respectively. In addition, the decline phase showed the lowest total sites concentrations, which was largely attributed to the lack of phosphoric functional groups and the lower hydroxyl functional groups. Although the carboxyl and hydroxyl functional groups were involved in the Pb(II) binding as aforementioned, the lowest total sites concentrations caused the lowest biosorption capacity of Pb(II) biosorption.

It was noted that the total surface functional groups showed no significant differences between the biomass of logarithmic phase and stable phase. However, as for the effective active sites for Pb(II) binding, the carboxyl groups were found more in stable phase than that in logarithmic phase as stated in FT-IR and XPS analysis. Indeed, the extra effective carboxyl groups contributing to the Pb(II) binding at the stable growth stage (Fig. 5, 6 and Table 4) might be attributed to the presence of galacturonic acid on the surface of microalgal biomass,[14] which tended to increase with growth phase and decreased after stationary phase,[34] leading to the higher biosorption capacity of biomass from stable growth phase. Also, the higher

Table 5 Titration results of biosorbents calculated with Protofit (mol kg^{-1})^a

Growth phase	pK_1	C1	pK_2	C2	pK_3	C3	pK_4	C4	C$_{tot}$
Logarithmic phase	6.78 ± 0.11	0.19 ± 0.11	4.04 ± 0.06	0.39 ± 0.07	8.73 ± 0.15	0.21 ± 0.03	10.37 ± 0.09	2.95 ± 0.06	3.74 ± 0.05
Stable phase	6.61 ± 0.13	0.22 ± 0.08	3.98 ± 0.05	0.27 ± 0.08	8.78 ± 0.10	0.23 ± 0.06	9.79 ± 0.20	3.07 ± 0.10	3.79 ± 0.11
Decline phase	ND	ND	3.43 ± 0.06	0.15 ± 0.05	8.92 ± 0.08	0.22 ± 0.04	11.22 ± 0.21	1.81 ± 0.09	1.55 ± 0.14
Fundamental groups	Phosphoryl		Carboxyl		Amine		Hydroxyl		

^{a} ND: not detected.

concentration of hydroxyl and phosphoryl in the surface of biomass from stable phase than that from logarithmic phase further contributed to the larger Pb(II) biosorption capacity. Given that the algal cells of stable growth stage had the highest biomass concentration, it was recommended that stable phase biomass can be harvested as biosorbents for heavy metal removal.

4 Conclusions

The algal dry biomass from each growth phase represented highly efficient removal of Pb(II) from water with the highest Pb(II) biosorption capacity of 298.17 mg g^{-1} at stable phase. The experimental data were well fitted with the pseudo-second-order kinetics and Freundlich isotherm models. The FT-IR, XPS and PT analysis showed that the more effective active sites in carboxyl, and higher sites concentrations of hydroxyl and phosphoryl functional groups contributed to the largest biosorption capacity of biomass from stable phase. Thus, the stable phase biomass can be used as an efficient, and inexpensive and environment-friendly biosorbent for heavy metal removal.

Acknowledgements

References

1 M. V. Subbaiah, G. Yuvaraja, Y. Vijaya and A. Krishnaiah, *J. Taiwan Inst. Chem. Eng.*, 2011, **42**, 965–971.

2 Y. Liu, Q. Zhao, G. Cheng and H. Xu, *Chem. Eng. J.*, 2011, **173**, 792–800.

3 H. Chen, J. Zhao, G. Dai, J. Wu and H. Yan, *Desalination*, 2010, **262**, 174–182.

4 A. Çelekli, M. Yavuzatmaca and H. Bozkurt, *J. Hazard. Mater.*, 2010, **173**, 123–129.

5 F. V. Hackbarth, F. Girardi, S. M. A. G. U. de Souza, A. A. U. de Souza, R. A. R. Boaventura and V. J. P. Vilar, *Chem. Eng. J.*, 2013, **242**, 294–305.

6 D. Bulgariu and L. Bulgariu, *Bioresour. Technol.*, 2012, **103**, 489–493.

7 M. Mohan and S. K. Dubey, *Ecotoxicol. Environ. Saf.*, 2013, **98**, 1–7.

8 L. Bulgariu, M. Lupea, D. Bulgariu, C. Rusu and M. Macoveanu, *Environ. Eng. Manage. J.*, 2013, **12**, 183–190.

9 D. Bulgariu and L. Bulgariu, *J. Cleaner Prod.*, 2015, 1–9.

10 J. He, A. Liu and J. Paul Chen, *J. Colloid Interface Sci.*, 2015, **439**, 162–169.

11 R. Y. Stanier, R. Kunisawa, M. Mandel and G. Cohen-Bazire, *Bacteriol. Rev.*, 1971, **35**, 171–205.

12 M. K. Ji, R. A. I. Abou-Shanab, S. H. Kim, E. S. Salama, S. H. Lee, A. N. Kabra, Y. S. Lee, S. Hong and B. H. Jeon, *Ecological Engineering*, 2013, **58**, 142–148.

13 W. Peng, H. Li, Y. Liu and S. Song, *J. Mol. Liq.*, 2016, **221**, 82–87.

14 S. Hadjoudja, V. Deluchat and M. Baudu, *J. Colloid Interface Sci.*, 2010, **342**, 293–299.

15 L. Xia, H. Li and S. Song, *J. Appl. Phycol.*, 2016, **28**, 391–407.

16 X. Zhang, P. Amendola, J. C. Hewson, M. Sommerfeld and Q. Hu, *Bioresour. Technol.*, 2012, **116**, 477–484.

17 H. B. Senturk, D. Ozdes and C. Duran, *Desalination*, 2010, **252**, 81–87.

18 N. Masoudzadeh, F. Zakeri, T. b. Lotfabad, H. Sharafi, F. Masoomi, H. S. Zahiri, G. Ahmadian and K. A. Noghabi, *J. Hazard. Mater.*, 2011, **197**, 190–198.

19 U. F. Umar, M. A. Khan, M. Athar and J. A. Kozinski, *Chem. Eng. J.*, 2011, **171**, 400–410.

20 N. Barka, M. Abdennouri, A. Boussaoud and M. EL Makhfouk, *Desalination*, 2010, **258**, 66–71.

21 F. Deniz and S. D. Saygideger, *Bioresour. Technol.*, 2010, **101**, 5137–5143.

22 Y. Zhou, P. Lu and J. Lu, *Carbohydr. Polym.*, 2012, **88**, 502–508.

23 T. Y. Jiang, J. Jiang, R. K. Xu and Z. Li, *Chemosphere*, 2012, **89**, 249–256.

24 P. Sarwa and S. K. Verma, *Clean: Soil, Air, Water*, 2014, **42**, 1298–1303.

25 G. Blázquez, M. A. Martín-Lara, E. D. Ruiz, G. Tenorio and M. Calero, *J. Ind. Eng. Chem.*, 2012, **18**, 1741–1750.

26 M. Mecozzi, M. Pietroletti and A. Tornambé, *Spectrochim. Acta, Part A*, 2011, **78**, 1572–1580.

27 H. Cui, J. Chen, H. Yang, W. Wang, Y. Liu, D. Zou, W. Liu and G. Men, *Chem. Eng. J.*, 2013, **232**, 372–379.

28 C. Bertagnolli, A. Uhart, J. C. Dupin, M. G. C. da Silva, E. Guibal and J. Desbrieres, *Bioresour. Technol.*, 2014, **164**, 264–269.

29 P. Sun, C. Hui, S. Wang, L. Wan, X. Zhang and Y. Zhao, *Colloids Surf., B*, 2016, **139**, 164–170.

30 X. Xu, A. Schierz, N. Xu and X. Cao, *J. Colloid Interface Sci.*, 2016, **463**, 55–60.

31 J. Wu, C. Jin, Z. Yang, J. Tian and R. Yang, *Carbon*, 2015, **82**, 562–571.

32 Z. Zheng, L. Qiang, T. Yang, B. Wang, X. Cui and H. Wang, *J. Polym. Res.*, DOI: 10.1007/s10965-014-0443-2.

33 F. Xiao, K. Wang and M. S. Zhan, *J. Mater. Sci.*, 2012, **47**, 4904–4913.

34 R. L. Soon, R. L. Nation, S. Cockram, J. H. Moffatt, M. Harper, B. Adler, J. D. Boyce, I. Larson and J. Li, *J. Antimicrob. Chemother.*, 2011, **66**, 126–133.